Random critical point separates brittle and ductile yielding transitions in amorphous materials

Misaki Ozawa[a,1], Ludovic Berthier[a,1,2], Giulio Biroli[b,c,1], Alberto Rosso[d,1], and Gilles Tarjus[e,1]

[a]Laboratoire Charles Coulomb (L2C), Université de Montpellier, CNRS, 34095 Montpellier, France; [b]Institut de Physique Théorique, Université Paris Saclay, Commissariat à l'énergie atomique (CEA), CNRS, F-91191 Gif-sur-Yvette, France; [c]Laboratoire de Physique Statistique, École Normale Supérieure, CNRS, Paris Sciences et Lettres (PSL) Research University, Sorbonne Université, 75005 Paris, France; [d]Laboratoire de Physique Théorique et Modèles Statistiques (LPTMS), CNRS, Université Paris-Sud, Université Paris-Saclay, 91405 Orsay, France; and [e]Laboratoire de Physique Théorique de la Matière Condensée, CNRS UMR 7600, Université Pierre et Marie Curie (UPMC)-Sorbonne Université, 75252 Paris Cedex 05, France

Edited by Pablo G. Debenedetti, Princeton University, Princeton, NJ, and approved May 9, 2018 (received for review April 10, 2018)

We combine an analytically solvable mean-field elasto-plastic model with molecular dynamics simulations of a generic glass former to demonstrate that, depending on their preparation protocol, amorphous materials can yield in two qualitatively distinct ways. We show that well-annealed systems yield in a discontinuous brittle way, as metallic and molecular glasses do. Yielding corresponds in this case to a first-order nonequilibrium phase transition. As the degree of annealing decreases, the first-order character becomes weaker and the transition terminates in a second-order critical point in the universality class of an Ising model in a random field. For even more poorly annealed systems, yielding becomes a smooth crossover, representative of the ductile rheological behavior generically observed in foams, emulsions, and colloidal glasses. Our results show that the variety of yielding behaviors found in amorphous materials does not necessarily result from the diversity of particle interactions or microscopic dynamics but is instead unified by carefully considering the role of the initial stability of the system.

amorphous solids | yielding transition | rheology

In amorphous solids, yielding generically signals a macroscopic change of the global mechanical response from an apparent elastic–solid regime at small deformation to a plastic–flow regime at large deformation (1–3). Yielding can occur smoothly, as when one spreads cream cheese on a bagel, or can be abrupt and catastrophic, as when a smartphone screen breaks. Yielding is observed in soft glasses such as emulsions, colloidal suspensions, and foams (1) but also in molecular and metallic glasses (3). It represents a central problem in statistical physics (2) (Can yielding be described as a nonequilibrium phase transition?), soft condensed matter (1) (How do soft glasses flow?), and materials science (3) (Can one predict material failure?). Understanding the fate of an amorphous material that is mechanically driven very slowly from an initial disordered configuration represents the core challenge, and its solution would directly allow one to understand steady-state flows (1), oscillatory deformations (4), shear-band formation (5), and perhaps most importantly, the catastrophic failure of amorphous solids (3).

Failure and flow of a disordered solid is such a ubiquitous phenomenon in nature and technological applications that it has stimulated an intensive search for universal explanations (6–8). One such explanation is based on elasto-plastic models (2, 9–11) and their analogy with the depinning of a manifold in a random environment (12, 13); it has recently allowed a clarification of the critical nature of the steady-flow regime observed at very large deformation. In this stationary regime, the stress undergoes a succession of elastic charges interrupted by sudden plastic drops. Microscopically, plasticity corresponds to localized particle rearrangements, called shear transformations (14, 15), which release the accumulated stress and induce long-range reorganization triggering system-spanning avalanches. Universality emerges because the stress drops display scale-free statistics, similar to the Gutenberg–Richter law for earthquakes (12, 13, 16–19).

The above studies are focused on "ductile" rheological responses observed in most soft glassy materials (such as cream cheese), which do reach a steady state. However, many amorphous solids (such as smartphone screens) are instead "brittle" and fail macroscopically after a finite deformation. For both ductile and brittle materials, the nature of the yielding transition between an elastic-like and a plastic behavior is an actively studied and vigorously debated question. Different views have been proposed. Yielding has been first described as a spinodal (i.e., a limit of stability) in ref. 20 on the basis of random first-order transition theory. Later, in agreement with infinite dimensional computations (21–23), yielding has been interpreted as a discontinuous transition (24) and then, later on, associated to a critical spinodal (25), independently of the initial preparation. In addition to the specific characterization of the yielding transition, a crucial open question is why, despite their strong structural similarities, are some materials brittle and others ductile?

Here we show that yielding and brittleness are two facets of the same problem, which we describe at once.* We provide a theoretical and numerical analysis of the transient response

Significance

Understanding how amorphous solids yield in response to external deformations is crucial both for practical applications and for theoretical reasons. Here we show that despite large differences in the materials' microscopic interactions, a degree of universality emerges as there are only two ways in which amorphous solids respond to a deformation: One, typical of well-annealed materials, is characterized by an abrupt failure with a macroscopic stress drop and the sudden emergence of sharp shear bands; the other, typical of poorly annealed materials, shows merely a smooth crossover. By varying the preparation protocol, one can change the response of a given material from one to the other, and this change is controlled by a random critical point.

Author contributions: M.O., L.B., G.B., A.R., and G.T. designed research, performed research, analyzed data, and wrote the paper.

The authors declare no conflict of interest.

This article is a PNAS Direct Submission.

[1]M.O., L.B., G.B., A.R., and G.T. contributed equally to this work.

[2]To whom correspondence should be addressed. Email: ludovic.berthier@umontpellier.fr.

This article contains supporting information online at www.pnas.org/lookup/suppl/doi:10.1073/pnas.1806156115/-/DCSupplemental.

Published online June 11, 2018.

*In this paper we use the term brittle to characterize a discontinuous yielding. Although this phenomenon is not accompanied by the formation of regions of vacuum, as it happens in the fracture of brittle materials, the macroscopic avalanche taking place at the discontinuous yielding transition does resemble a crack induced by a brittle fracture. In this sense, the behavior at discontinuous yielding is brittle-like.

to an athermal shear deformation starting from the disordered solid. Our main finding is that there are two different universal behaviors, depending on the degree of annealing of the initial configuration but not on the detailed nature of the material per se. We show that the evolution of the stress caused by quasi-static deformations qualitatively changes from a sharp discontinuous transition when the material is initially well annealed, and therefore very stable, to a smooth crossover as the degree of annealing decreases and the material is initially less stable. These two regimes are separated by a random critical point, by which we denote a critical point controlled by the presence of quenched disorder. It is reached for a critical value of the degree of annealing. Our analysis suggests that this criticality is related to the universality class of an Ising model in a random field [generically denoted by RFIM (26)]. In this picture, the yielding of ductile materials, which are viewed as rather poorly annealed systems, does not correspond to a genuine phase transition.

The starting point of our work is the idea, inspired by random first-order transition theory (20) and mean-field calculations (21–23), that yielding corresponds to a spinodal instability, but we additionally take into account several important features that can change the picture drastically: (*i*) the presence of quenched disorder, physically corresponding to the intrinsic structural heterogeneity present in amorphous materials; (*ii*) the possible disappearance of the spinodal that can be replaced by a smooth crossover; and (*iii*) finite-dimensional fluctuations, which are generically expected to destroy the criticality associated to a mean-field spinodal instability. In the following, we first support our claims by studying an analytically solvable mean-field elasto-plastic model that we devise to capture the brittle-to-ductile transition through a random critical point. We then use molecular dynamics simulations of a glass-former prepared over an unprecedented range of initial stability, building on very recent computational developments (27). The simulations fully confirm the theoretical scenario and provide direct evidence for a random critical point controlling the brittleness of amorphous solids.

Mean-Field Theory

To substantiate our proposal, we develop a simple analysis, which is inspired by the description of sheared materials in terms of elasto-plastic models (2). This widespread mesoscopic approach successfully reproduces the key phenomenology of deformation and flow in amorphous materials. Our main focus is on the role of the initial preparation, which has received much less attention (see, however, refs. 28–31).

In this approach, the system is decomposed in mesoscopic blocks $i=1,\cdots,N_{\rm b}$, in which elastic behavior is interrupted by sudden shear transformations. At each block is assigned a local stress, σ_i, drawn from an initial distribution $P_{\rm ini}(\sigma)$, which encodes the degree of annealing. In the absence of plastic events, the response is purely elastic, and a small deformation increment, $\delta\gamma$, loads all of the blocks as $\sigma_i\to\sigma_i+2\mu_2\delta\gamma$, with μ_2 the shear modulus. However, when the local stress becomes larger than a threshold value $\sigma_i^{\rm th}$ (that for simplicity we consider uniform $\sigma_i^{\rm th}=\sigma^{\rm th}$), the block yields and the local stress drops by a random quantity $x\geq 0$ sampled from a given distribution $g(x)$. After the drop, the stress is redistributed to the other sites as $\sigma_j\to\sigma_j+\mathcal{G}_{ij}x$. The elastic kernel $\mathcal{G}_{ij}$ is generally taken of the Eshelby form, which corresponds to the far-field solution of elasticity (it decays as $1/|i-j|^d$, where d is the spatial dimension, but changes sign and displays a quadrupolar symmetry) (32). There is no straightforward and generally accepted way to handle the nonlocal Eshelby interaction kernel at a mean-field level (33–35). Here we consider a mean-field approximation that consists of replacing this nonlocal interaction by a fully connected kernel $\mathcal{G}_{ij}=\frac{\mu_2}{N_{\rm b}(\mu_1+\mu_2)}$, with $\mu_1>0$. This description overlooks the effect of the anisotropic and nonpositive form of the Eshelby interaction kernel. Nonetheless, we expect that it provides a correct qualitative description of the yielding transition itself. [A similar behavior is indeed found by analyzing more involved mean-field models (36).] Below we discuss its limitations and how to go beyond them. Note that this model also has a natural interpretation as a mean-field model of depinning[†] as well as earthquake statistics (38, 39).

The key quantity in this approach is the distribution $P_\gamma(x)$ of the distances $x_i=\sigma^{\rm th}-\sigma_i$ from the threshold stress. In the following, we study its macroscopic evolution with strain γ. As detailed in *SI Appendix*, it is governed by the equation

$$\frac{\partial P_\gamma(x)}{\partial\gamma}=\frac{2\mu_2}{1-x_cP_\gamma(0)}\left[\frac{\partial P_\gamma(x)}{\partial x}+P_\gamma(0)g(x)\right], \qquad [1]$$

where $x_c=(\mu_2/[\mu_1+\mu_2])\bar{x}$ and $\bar{x}=\int_0^\infty dx x g(x)$ represent material-dependent parameters (here, we have $x_c<\bar{x}<1$ as we set $\sigma^{\rm th}=1$ as the stress unit). The degree of annealing of the material is fully encoded in the initial distribution $P_{\gamma=0}(x)$, which contains the same information as $P_{\rm ini}(\sigma)$.

The properties of the macroscopic stress–strain curves can be obtained through Eq. **1** and the relation $\langle\sigma\rangle=1-\langle x\rangle$, which is derived by taking the average of the equation defining x_i. Our results, which hold for a generic $g(x)$ (see *SI Appendix*), are shown in Fig. 1 for the explicit case $g(x)=\exp(-x/\bar{x})/\bar{x}$ and $P_{\gamma=0}(x)=\left(e^{-x/A}-e^{-x/(1-A)}\right)/(2A-1)$, $1/2<A<1$. With this choice, A is the unique parameter controlling the degree of annealing, with smaller values of A corresponding to better annealed samples.

For a poor annealing, the stress–strain curve is monotonically increasing and yielding is a mere crossover. As one increases the degree of annealing, a stress overshoot first appears, but yielding remains a crossover, still not a bona fide phase transition. For the best annealing, the overshoot is followed by a spinodal and a sharp discontinous jump of the average stress. Mathematically, this occurs when, increasing γ, $P_\gamma(0)$ reaches x_c^{-1}, thus inducing a singular behavior of $P_\gamma(x)$ via Eq. **1**. In this case, yielding takes place as a nonequilibrium first-order transition. Crucially, a critical point A_c separates the first-order regime from the smooth one. From Fig. 1, it is clear that an appropriate order parameter distinguishing the two regimes of yielding is the macroscopic stress drop $\Delta\langle\sigma\rangle$. As shown in Fig. 1, *Inset*, $\Delta\langle\sigma\rangle$ vanishes at large A, but it grows continuously by decreasing A below A_c. This critical point is therefore reached not only for a specific value of the strain and stress but also by tuning the degree of annealing of the material. The stress overshoot, frequently observed in colloidal materials (40, 41), yield stress fluids (42), and computer simulations (43), is simply a vestige of this critical point at larger disorder strength.

When a spinodal, followed by a discontinuity, is present, the stress displays a square-root singularity as the yield strain γ_Y is approached from below, and the distribution of the avalanche size S becomes for large S

$$\langle\sigma\rangle-\sigma_{\rm sp}\propto(\gamma_Y-\gamma)^{1/2}, \qquad [2]$$

$$\mathcal{P}(S)\sim S^{-3/2}e^{-C(\gamma_Y-\gamma)S}, \qquad [3]$$

where $C>0$ is a constant and $\gamma\to\gamma_Y^-$. The discontinuous stress drop decreases as annealing becomes poorer, and it eventually

[†]A narrower initial distribution, different from the stationary one, corresponds to aging in the quenched disordered (28, 37)—that is, to a stronger pinning at initial times.

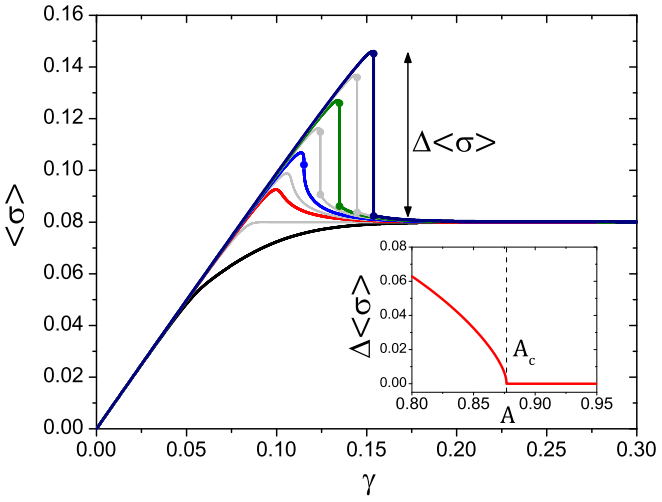

Fig. 1. The different yielding regimes in the mean-field elasto-plastic model. Stress $\langle\sigma\rangle$ versus strain γ for increasing degree of annealing (decreasing A values) from bottom to top, using $x_c = 0.9, \bar{x} = 0.92$. The monotonic flow curve (black) transforms into a smooth stress overshoot (red), and above a critical point with infinite slope (blue) becomes a discontinuous transition (green) of increasing amplitude (dark blue). (*Inset*) Stress discontinuity $\Delta\langle\sigma\rangle$ versus the degree of annealing [here, the initial distribution $P_{\gamma=0}(x)$ is parametrized by a single parameter A, which plays the same role as the preparation temperature in the simulations].

vanishes with a square-root singularity at the critical point (γ_{Y_c}, σ_c), where a different behavior emerges:

$$\langle\sigma\rangle - \sigma_c \propto \mathrm{sgn}(\gamma - \gamma_{Y_c})|\gamma - \gamma_{Y_c}|^{1/3}, \quad [4]$$

$$\mathcal{P}(S) \sim S^{-3/2} e^{-C'|\gamma-\gamma_{Y_c}|^{4/3}S}, \quad [5]$$

with $C' > 0$ and $\gamma \to \gamma_{Y_c}^{\pm}$. All these scaling behaviors coincide with those found for the RFIM[‡] within the mean-field theory (45).

The presence of an annealing-controlled random critical point is the main finding of our mean-field approach. We stress that its presence, as well as that of the different regimes of yielding, does not require the introduction of any additional physical mechanism, such as dynamical weakening (37–39, 46–48). It only depends on the initial preparation of the amorphous material before shearing, in combination with the basic rules of elasto-plastic models. In finite dimensions, the above scaling behaviors will be modified. Whereas a spinodal instability can still be present in athermal conditions, it will likely not be associated to any critical behavior (49). On the other hand, the random critical point should always be in the universality class of the athermally driven RFIM, but this class is presumably distinct from that of the conventional model with only short-ranged ferromagnetic interactions.

This mean-field description is not meant to reproduce all aspects of the deformation-and-flow phenomenology. In particular, it does not allow criticality of the sheared system along the elastic and plastic branches (29, 50), nor can it describe spatial flow inhomogeneities, such as shear bands. Nonetheless, as we now show by computer simulations, the model correctly captures the preparation dependence of the yielding transition, the central question addressed by our work.

[‡]More precisely, in the present context, one should consider the out-of-equilibrium behavior of the RFIM when quasi-statically driven at zero temperature by a change of the applied magnetic field (44). At the mean-field level, this critical behavior is the same as that of the RFIM in equilibrium.

Atomistic Model and Numerical Procedures

We have numerically studied the yielding transition in a 3D atomistic glass model for different degrees of annealing, with our mean-field predictions as a guideline. We have used a size-polydisperse model with a soft repulsive potential (27). Glass samples have been prepared by first equilibrating liquid configurations at a finite temperature, T_{ini}, and then performing a rapid quench to $T = 0$, the temperature at which the samples are subsequently deformed. The preparation temperature T_{ini} then uniquely controls the glass stability, and we consider a wide range of preparation temperatures, $T_{\mathrm{ini}} = 0.062 - 0.200$. To obtain well-annealed systems, we have used the swap Monte Carlo (SWAP) algorithm, which allows equilibration at extremely low temperatures (27). The considered range of T_{ini} describes very poorly annealed glasses ($T_{\mathrm{ini}} \approx 0.2$, corresponding to wet foam experiments), ordinary computer glasses ($T_{\mathrm{ini}} \approx 0.12$, corresponding to colloidal experiments), well-annealed glasses ($T_{\mathrm{ini}} \approx 0.085 - 0.075$, corresponding to metallic-glass experiments), as well as ultrastable glasses ($T_{\mathrm{ini}} \approx 0.062$, see ref. 51). No previous numerical work has ever accessed such a large range of glass stability.

We have performed strain-controlled athermal quasi-static shear (AQS) deformation using Lees–Edwards boundary conditions (18). Note that during the AQS deformation, the system is always located in a potential energy minimum, such that inertia and thermal fluctuations play no role. This method is considered as the zero-strain rate limit, $\dot{\gamma} \to 0$, which bypasses the time scale gap between simulation and experiments (43). Thus, our simulation setting (SWAP/AQS) fully overcomes the time scale gap in both glass preparation and mechanical deformation between simulations and experiments. To study the finite-size effect, we have varied the number of particles N over a considerable range, $N = 1500 - 96000$. More details are given in *SI Appendix*.

The Two Regimes of Yielding

In Fig. 2*A*, we show the evolution of typical stress–strain curves for large individual samples with $N = 96000$. For a high T_{ini}, the usual jerky succession of stress drops is found with no overshoot for $T_{\mathrm{ini}} = 0.200$ [akin to wet foam experiments (52, 53)] and with a stress overshoot for $T_{\mathrm{ini}} = 0.120$ [akin to colloids experiments (40, 41)]. Note that previous simulation studies about effects of annealing on yielding behavior would be restricted by this regime (43, 54, 55). Strikingly, the stress overshoot transforms into a sharp stress discontinuity for $T_{\mathrm{ini}} \lesssim 0.1$ near the yield strain $\gamma_Y \approx 0.12$. This large stress drop is distinct from the smaller stress drops observed at other strain values. This is confirmed in Fig. 2*D*, where we plot for increasing values of N the averaged stress $\langle\sigma\rangle$ (obtained by averaging over many independent samples) for $T_{\mathrm{ini}} = 0.062$. The stress discontinuity at yielding is the only one surviving after the average and it becomes sharper and better resolved as N increases. These data strongly suggest that, in the thermodynamic limit, the averaged stress–strain curve has a sharp discontinuity at yielding and is smooth everywhere else. This discontinuity is a signature of a nonequilibrium first-order transition, as confirmed by the growth of the associated susceptibilities, the so-called "connected" susceptibility $\chi_{\mathrm{con}} = -\frac{d\langle\sigma\rangle}{d\gamma}$ and "disconnected" susceptibility $\chi_{\mathrm{dis}} = N(\langle\sigma^2\rangle - \langle\sigma\rangle^2)$. The peaks of the susceptibilities become sharper and their amplitude, $\chi_{\mathrm{con}}^{\mathrm{peak}}$ and $\chi_{\mathrm{dis}}^{\mathrm{peak}}$, increases with N with exponents expected for a first-order transition in the presence of quenched disorder, as discussed below. This is illustrated for χ_{dis} in Fig. 2*E*, and we find that $\chi_{\mathrm{dis}}^{\mathrm{peak}} \sim N$ (*Inset*) and $\chi_{\mathrm{con}}^{\mathrm{peak}} \sim \sqrt{N}$ (see *SI Appendix*) at large N.

The similarity between the mean-field theory in Fig. 1 and the data in Fig. 2*A* is patent. In agreement with the mean-field theory, we indeed find two distinct types of yielding: a

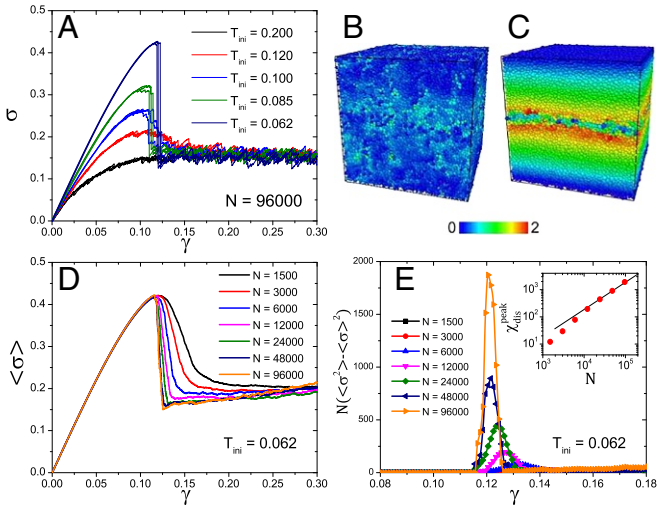

Fig. 2. From ductile to brittle behavior. (*A*) The yielding regimes in the simulation of a sheared glass for different degrees of annealing. Shown is stress σ as a function of the strain γ for several preparation temperatures T_{ini}. For each T_{ini}, three independent samples are shown. (*B* and *C*) Snapshots of nonaffine displacements between $\gamma = 0$ and yielding at $\gamma = 0.13$ for $T_{\text{ini}} = 0.120$ (*B*) and at $\gamma = 0.119$ for $T_{\text{ini}} = 0.062$ (*C*). (*D* and *E*) Evidence of a first-order yielding transition for well-annealed glasses. Shown is a system-size dependence of the averaged stress–strain curve for $T_{\text{ini}} = 0.062$, showing a sharper stress drop for larger N (*D*). The associated susceptibility, $\chi_{\text{dis}} = N(\langle\sigma^2\rangle - \langle\sigma\rangle^2)$, becomes sharper as N increases (*E*). (*Inset*) The divergence of the maximum of χ_{dis} is proportional to N shown with the straight line.

discontinuous one for well-annealed glasses, which is associated with a first-order transition that becomes weaker as the degree of annealing decreases, and a continuous one, corresponding to a smooth crossover, for poorly annealed materials. As discussed in the next section, we also find a critical point at $T_{\text{ini},c} \approx 0.095$ that marks the limit between the two regimes.

In addition, the simulations give direct real-space insight into the nature of yielding. We illustrate the prominent difference between the two yielding regimes in the snapshots of nonaffine displacements measured at yielding in Fig. 2 *B* and *C* (see *SI Appendix* for corresponding movies). For a smooth yielding, we find in Fig. 2*B* that the nonaffine displacements gradually fill the box as γ increases, and concomitantly the stress displays an overshoot, as recently explored (56, 57). For the discontinuous case, the sharp stress drop corresponds to the sudden emergence of a system spanning shear band. By contrast with earlier work on shear-banding materials (58, 59), the shear band in Fig. 2*C* appears suddenly in a single infinitesimal strain increment and does not result from the accumulation of many stress drops at large deformation. For an intermediate regime between the discontinuous and continuous yielding ($T_{\text{ini}} \approx 0.1$), strong sample-to-sample fluctuations are observed. Some samples show a sharp discontinuous yielding with a conspicuous shear band (similar to Fig. 2*C*), whereas other samples show smooth yielding with rather homogeneous deformation (similar to Fig. 2*B*). Such large sample-to-sample fluctuations are typical for systems with random critical points.

The Random Critical Point

Having identified a regime where yielding takes place through a first-order discontinuity and a regime where it is a smooth crossover, we now provide quantitative support for the existence of a critical point separating them, as one would indeed expect on general grounds. The mean-field theory presented above supports this scenario and suggests that the critical point is in the universality class of an Ising model in a random field. This criticality should not be confused with the marginality predicted to be present in sheared amorphous solids irrespective of the degree of annealing and of the value of the strain (29, 50). This issue is discussed separately below and in *SI Appendix*.

As shown in Fig. 1, the order parameter distinguishing the two regimes of yielding is the macroscopic stress drop. In the simulations, we measure its evolution by recording for each sample the maximum stress drop $\Delta\sigma_{\text{max}}$ observed in the strain window $\gamma \in [0, 0.3]$. We have measured the mean value $\langle\Delta\sigma_{\text{max}}\rangle$ as a function of the preparation temperature T_{ini} for several system sizes N. At the largest temperature, no macroscopic stress drop exists: $\langle\Delta\sigma_{\text{max}}\rangle$ simply reflects stress drops along the plastic branch and vanishes as $\langle\Delta\sigma_{\text{max}}\rangle|_{T_{\text{ini}}=0.2} \sim N^{-0.4}$, as shown in Fig. 3*A*, *Inset*. In the main panel of Fig. 3*A*, we subtract this trivial behavior from $\langle\Delta\sigma_{\text{max}}\rangle$. We find that the maximum stress drop is zero above $T_{\text{ini}} \approx 0.1$ and nonzero for lower temperatures. The system-size dependence confirms that this temperature evolution becomes crisp in the large-N limit, and we locate the critical point at $T_{\text{ini},c} \approx 0.095$. Complementary information is provided by studying the fluctuations of the maximum stress drop, which can be quantified through their variance $N(\langle\Delta\sigma^2_{\text{max}}\rangle - \langle\Delta\sigma_{\text{max}}\rangle^2)$ [not to be confused with the disconnected susceptibility $\chi_{\text{dis}} = N(\langle\sigma^2\rangle - \langle\sigma\rangle^2)$], shown in Fig. 3*B*. One finds that the variance

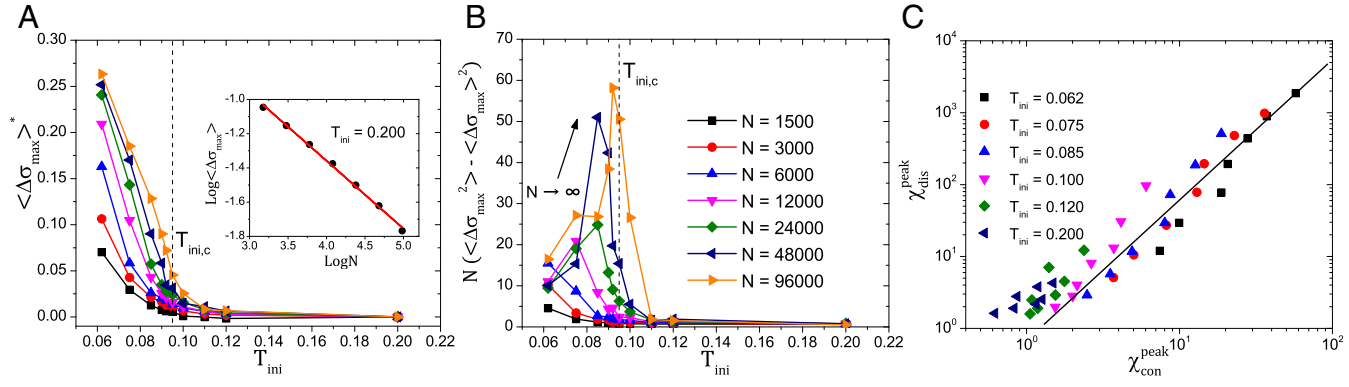

Fig. 3. Evidence of a random critical point. Mean (*A*) and variance (B) of $\Delta\sigma_{\text{max}}$ versus the preparation temperature T_{ini} for several system sizes N. In *A*, we plot $\langle\Delta\sigma_{\text{max}}\rangle^* \equiv \langle\Delta\sigma_{\text{max}}\rangle - \langle\Delta\sigma_{\text{max}}\rangle|_{T_{\text{ini}}=0.2}$ to subtract the trivial high-temperature dependence that vanishes at large N, as shown in *Inset*. The critical temperature $T_{\text{ini},c} \approx 0.095$ is determined from the vanishing of the order parameter $\langle\Delta\sigma_{\text{max}}\rangle^*$ in *A* and the growth of the maximum of the susceptibility $N(\langle\Delta\sigma^2_{\text{max}}\rangle - \langle\Delta\sigma_{\text{max}}\rangle^2)$ in *B*. (*C*) Parametric plot of the connected and disconnected susceptibilities for all system sizes and several preparation temperatures. The straight line corresponds to the scaling $\chi_{\text{dis}} \propto \chi^2_{\text{con}}$, as found in the RFIM.

goes through a maximum that increases with system size around $T_{\mathrm{ini},c} \approx 0.095$.

These results provide strong evidence of a critical point separating ductile from brittle behavior, with the mean stress drop $\langle \Delta\sigma_{\max} \rangle$ playing the role of an order parameter. Additional support comes from the study of the overlap function q introduced in ref. 24. We find that the finite-size analysis of q and of the overlap jump $\Delta q_{\max}$ at yielding follows the same pattern as σ and $\Delta\sigma_{\max}$ qualitatively. This points toward a macroscopic discontinuity for well-annealed glasses and a mere crossover for poorly annealed cases (see *SI Appendix*). Contrary to what was found in ref. 60, we find that the first-order transition behavior terminates at a temperature $T_{\mathrm{ini},c}$, above which a smooth stress overshoot is instead observed.

Our findings are also corroborated by the analysis of the criticality of the sheared glass. As previously shown (29, 61), an amorphous material quasi-statically sheared at zero temperature is marginal at all values of the strain. The physical reason is the presence of a pseudogap in the density of elementary excitation (50), which is characterized by a critical exponent $\theta > 0$. This criticality implies a scale-free distribution of avalanche sizes, and by carefully analyzing the stress-drop statistics, we have extracted the exponent θ as a function of γ and T_{ini}. As shown in *SI Appendix*, we find that the discontinuous transition is associated with a discontinuous variation of θ and that large fluctuations of the stress drops associated with criticality generate a rapid change in θ versus γ with the presence of a large maximum for temperatures T_{ini} close to the critical point.

Our data do not allow us to measure the critical exponents associated to the RFIM critical point in a robust way. Yet it is possible to obtain a strong indication that the critical point and the first-order transition are governed by the universality class of an Ising model in a random field. In this case indeed, the presence of quenched disorder leads to two distinct susceptibilities, χ_{con} and χ_{dis}. A key signature of the presence of random-field disorder is that $\chi_{\mathrm{dis}} \propto \chi_{\mathrm{con}}^2$. This scaling relation, which is exact in the mean-field limit, is valid in finite dimensions at the first-order transition and is also approximately verified by the conventional RFIM at the critical point (26). It indicates that disorder-induced sample-to-sample fluctuations provide the dominant source of fluctuations. By looking at the parametric plot of the maximum of χ_{dis} versus the maximum of χ_{con}, which is shown in Fig. 3*C* for all system sizes and several preparation temperatures, one finds that the relation is indeed observed in our simulations, at least at and below a temperature $T_{\mathrm{ini}} = 0.100 \gtrsim T_{\mathrm{ini},c}$ and for large N.

Discussion and Conclusion

Our analysis shows that irrespective of the nature of the amorphous material, yielding can come with two qualitatively different types of behavior, corresponding either to a discontinuous transition or to a smooth crossover. The transition between these two regimes occurs at a random critical point related to the RFIM, which naturally explains the large sample-to-sample fluctuations observed in simulations. The type of yielding that a given material displays depends on its degree of annealing, a mechanism that differs dramatically from the processes at play in crystalline solids (62). Conceptually, increasing the annealing for a given particle interaction implies that the initial amorphous configuration is drawn from a deeper location of the glassy energy landscape, in which the local environments fluctuate less (lower disorder in the RFIM analogy). In practice, the degree of annealing can be tuned for some materials such as metallic and molecular glasses (48, 63–65) but would be more difficult to vary for others like emulsions and wet foams. Our approach shows that given the particle size (for colloids), the preparation protocol (for emulsions), and the cooling rate (for metallic glasses), a given amorphous material must belong to either one of the two yielding regimes. We suggest that colloids with a well-chosen range of particle sizes could be used to experimentally probe the random critical point separating the two yielding regimes.

Our work is focused on the two possible yielding scenarios rather than on the stationary state reached at large deformation. In ductile glasses, one expects a stationary state independent of the initial condition as shear transformations are quickly healed so that plasticity can spread homogeneously. In the materials we dubbed brittle in the present work, large deformations would trigger cracks or shear bands that may remain well-localized in the sample (as we indeed find numerically). Our study does not allow us to study the propagation of the cracks themselves.

There are several directions worth further studies to extend our results. On the theoretical side it is important to introduce nonlocal elastic interactions mediated by an Eshelby-like kernel in the proposed framework of an effective random-field Ising theory, which could potentially yield anisotropic avalanches that are not described by the traditional RFIM. This is essential to describe the role of nonperturbative and non-mean field effects that have been argued to be important for the spinodal behavior of disordered finite-dimensional systems at zero temperature (49). These correspond physically to rare regions that are able to trigger the failure in the material and are related to the shear bands found in simulations. We present numerical evidence already supporting this scenario in *SI Appendix* (see also ref. 36). On the simulation side, it is interesting to study how the rheological setting affects the yielding scenario proposed in this work. Considering uniaxial tension or compression tests would be useful for a further detailed comparison between simulations and experiments. In addition, investigating the influence of a finite temperature and/or a finite strain rate on the simple situation studied here would also be a worthwhile extension. Finally, one would like to understand better how the evolution of ductility with the initial disorder impacts the deformation and failure of glasses at larger length scales and make a connection with studies of macroscopic fracture in glasses. Because controlling ductility in amorphous solids is desirable for practical applications (3, 66), our theoretical studies will hopefully lead to design-principle of more ductile glassy materials.

ACKNOWLEDGMENTS. We thank H. Ikeda, F. Landes, A. Nicolas, A Ninarello, I. Procaccia, G. Tsekenis, P. Urbani, M. Wyart, and F. Zamponi for helpful discussions. We thank A. Ninarello for sharing very low-temperature equilibrium configurations. This work is supported by Simons Foundation Grants 454933 (to L.B.) and 454935 (to G.B.).

1. Bonn D, Denn MM, Berthier L, Divoux T, Manneville S (2017) Yield stress materials in soft condensed matter. *Rev Mod Phys* 89:035005.
2. Nicolas A, Ferrero EE, Martens K, Barrat JL (2017) Deformation and flow of amorphous solids: A review of mesoscale elastoplastic models. arXiv:1708.09194.
3. Schuh CA, Hufnagel TC, Ramamurty U (2007) Mechanical behavior of amorphous alloys. *Acta Mater* 55:4067–4109.
4. Knowlton ED, Pine DJ, Cipelletti L (2014) A microscopic view of the yielding transition in concentrated emulsions. *Soft Matter* 10:6931–6940.
5. Greer A, Cheng Y, Ma E (2013) Shear bands in metallic glasses. *Mater Sci Eng R Rep* 74:71–132.
6. Perez-Reche F, Truskinovsky L, Zanzotto G (2008) Driving-induced crossover: From classical criticality to self-organised criticality. *Phys Rev Lett* 101: 230601.
7. Cubuk E, et al. (2017) Structure-property relationships from universal signatures of plasticity in disordered solids. *Science* 358:1033–1037.
8. Uhl JT, et al. (2015) Universal quake statistics: From compressed nanocrystals to earthquakes. *Sci Rep* 5:16493.
9. Picard G, Ajdari A, Lequeux F, Bocquet L (2004) Elastic consequences of a single plastic event: A step towards the microscopic modeling of the flow of yield stress fluids. *Eur Phys J E* 15:371–381.

10. Picard G, Ajdari A, Lequeux F, Bocquet L (2005) Slow flows of yield stress fluids: Complex spatiotemporal behavior within a simple elastoplastic model. *Phys Rev E* 71:010501.
11. Cao X, Nicolas A, Trimcev D, Rosso A (2018) Soft modes and strain redistribution in continuous models of amorphous plasticity: The Eshelby paradigm, and beyond? *Soft Matter* 14:3640–3651.
12. Lin J, Lerner E, Rosso A, Wyart M (2014) Scaling description of the yielding transition in soft amorphous solids at zero temperature. *Proc Natl Acad Sci USA* 111:14382–14387.
13. Baret JC, Vandembroucq D, Roux S (2002) Extremal model for amorphous media plasticity. *Phys Rev Lett* 89:195506.
14. Argon A, Kuo H (1979) Plastic flow in a disordered bubble raft (an analog of a metallic glass). *Mater Sci Eng* 39:101–109.
15. Falk ML, Langer JS (1998) Dynamics of viscoplastic deformation in amorphous solids. *Phys Rev E* 57:7192–7205.
16. Regev I, Weber J, Reichhardt C, Dahmen KA, Lookman T (2015) Reversibility and criticality in amorphous solids. *Nat Commun* 6:8805.
17. Salerno KM, Robbins MO (2013) Effect of inertia on sheared disordered solids: Critical scaling of avalanches in two and three dimensions. *Phys Rev E* 88:062206.
18. Maloney CE, Lemaître A (2006) Amorphous systems in athermal, quasistatic shear. *Phys Rev E* 74:016118.
19. Nicolas A, Rottler J, Barrat JL (2014) Spatiotemporal correlations between plastic events in the shear flow of athermal amorphous solids. *Eur Phys J E*. 37:50.
20. Wisitsorasak A, Wolynes PG (2012) On the strength of glasses. *Proc Natl Acad Sci USA* 109:16068.
21. Rainone C, Urbani P, Yoshino H, Zamponi F (2015) Following the evolution of hard sphere glasses in infinite dimensions under external perturbations: Compression and shear strain. *Phys Rev Lett* 114:015701.
22. Urbani P, Zamponi F (2017) Shear yielding and shear jamming of dense hard sphere glasses. *Phys Rev Lett* 118:038001.
23. Biroli G, Urbani P (2018) Liu-Nagel phase diagrams in infinite dimension. *SciPost Physics* 4:020.
24. Jaiswal PK, Procaccia I, Rainone C, Singh M (2016) Mechanical yield in amorphous solids: A first-order phase transition. *Phys Rev Lett* 116:085501.
25. Parisi G, Procaccia I, Rainone C, Singh M (2017) Shear bands as manifestation of a criticality in yielding amorphous solids. *Proc Natl Acad Sci USA* 114:5577–5582.
26. Nattermann T (1998) Theory of the random field Ising model. *Spin Glasses and Random Fields*, ed Young P (World Scientific, Singapore), pp 277–298.
27. Ninarello A, Berthier L, Coslovich D (2017) Models and algorithms for the next generation of glass transition studies. *Phys Rev X* 7:021039.
28. Vandembroucq D, Roux S (2011) Mechanical noise dependent aging and shear banding behavior of a mesoscopic model of amorphous plasticity. *Phys Rev B* 84:134210.
29. Lin J, Gueudré T, Rosso A, Wyart M (2015) Criticality in the approach to failure in amorphous solids. *Phys Rev Lett* 115:168001.
30. Vasoya M, Rycroft CH, Bouchbinder E (2016) Notch fracture toughness of glasses: Dependence on rate, age, and geometry. *Phys Rev Appl* 6:024008.
31. Liu C, Martens K, Barrat JL (2018) Mean-field scenario for the athermal creep dynamics of yield-stress fluids. *Phys Rev Lett* 120:028004.
32. Eshelby JD (1957) The determination of the elastic field of an ellipsoidal inclusion, and related problems. *Proceedings of the Royal Society of London A: Mathematical, Physical and Engineering Sciences*, ed Peierls RE (The Royal Society, London), Vol 241, pp 376–396.
33. Hébraud P, Lequeux F (1998) Mode-coupling theory for the pasty rheology of soft glassy materials. *Phys Rev Lett* 81:2934–2937.
34. Lemaitre A, Caroli C (2009) Rate-dependent avalanche size in athermally sheared amorphous solids. *Phys Rev Lett* 103:065501.
35. Lin J, Wyart M (2016) Mean-field description of plastic flow in amorphous solids. *Phys Rev X* 6:011005.
36. Popović M, de Geus TW, Wyart M (2018) Elasto-plastic description of brittle failure in amorphous materials. arXiv:1803.11504.
37. Jagla EA (2007) Strain localization driven by structural relaxation in sheared amorphous solids. *Phys Rev E* 76:046119.
38. Fisher DS, Dahmen K, Ramanathan S, Ben-Zion Y (1997) Statistics of earthquakes in simple models of heterogeneous faults. *Phys Rev Lett* 78:4885–4888.
39. Jagla EA, Landes FP, Rosso A (2014) Viscoelastic effects in avalanche dynamics: A key to earthquake statistics. *Phys Rev Lett* 112:174301.
40. Koumakis N, Laurati M, Egelhaaf S, Brady J, Petekidis G (2012) Yielding of hard-sphere glasses during start-up shear. *Phys Rev Lett* 108:098303.
41. Amann CP, et al. (2013) Overshoots in stress-strain curves: Colloid experiments and schematic mode coupling theory. *J Rheol* 57:149–175.
42. Divoux T, Barentin C, Manneville S (2011) Stress overshoot in a simple yield stress fluid: An extensive study combining rheology and velocimetry. *Soft Matter* 7:9335–9349.
43. Rodney D, Tanguy A, Vandembroucq D (2011) Modeling the mechanics of amorphous solids at different length scale and time scale. *Model Simul Mat Sci Eng* 19:083001.
44. Perković O, Dahmen K, Sethna JP (1995) Avalanches, Barkhausen noise, and plain old criticality. *Phys Rev Lett* 75:4528–4531.
45. Dahmen K, Sethna JP (1996) Hysteresis, avalanches, and disorder-induced critical scaling: A renormalization-group approach. *Phys Rev B* 53:14872.
46. Dahmen KA, Ben-Zion Y, Uhl JT (2009) Micromechanical model for deformation in solids with universal predictions for stress-strain curves and slip avalanches. *Phys Rev Lett* 102:175501.
47. Papanikolaou S, et al. (2012) Quasi-periodic events in crystal plasticity and the self-organized avalanche oscillator. *Nature* 490:517–521.
48. Coleman JP, et al. (2017) Effect of annealing on nanoindentation slips in a bulk metallic glass. *Phys Rev B* 96:134117.
49. Nandi SK, Biroli G, Tarjus G (2016) Spinodals with disorder: From avalanches in random magnets to glassy dynamics. *Phys Rev Lett* 116:145701.
50. Müller M, Wyart M (2015) Marginal stability in structural, spin, and electron glasses. *Annu Rev Condens Matter Phys* 6:177–200.
51. Fullerton CJ, Berthier L (2017) Density controls the kinetic stability of ultrastable glasses. *Europhys Lett* 119:36003.
52. Lauridsen J, Twardos M, Dennin M (2002) Shear-induced stress relaxation in a two-dimensional wet foam. *Phys Rev Lett* 89:098303.
53. Cantat I, Pitois O (2006) Stokes experiment in a liquid foam. *Phys Fluids* 18:083302.
54. Utz M, Debenedetti PG, Stillinger FH (2000) Atomistic simulation of aging and rejuvenation in glasses. *Phys Rev Lett* 84:1471–1474.
55. Fan M, et al. (2017) Effects of cooling rate on particle rearrangement statistics: Rapidly cooled glasses are more ductile and less reversible. *Phys Rev E* 95:022611.
56. Shrivastav GP, Chaudhuri P, Horbach J (2016) Yielding of glass under shear: A directed percolation transition precedes shear-band formation. *Phys Rev E* 94:042605.
57. Ghosh A, et al. (2017) Direct observation of percolation in the yielding transition of colloidal glasses. *Phys Rev Lett* 118:148001.
58. Shi Y, Falk ML (2005) Strain localization and percolation of stable structure in amorphous solids. *Phys Rev Lett* 95:095502.
59. Hassani M, Engels P, Raabe D, Varnik F (2016) Localized plastic deformation in a model metallic glass: A survey of free volume and local force distributions. *J Stat Mech Theor Exp* 2016:084006.
60. Procaccia I, Rainone C, Singh M (2017) Mechanical failure in amorphous solids: Scale-free spinodal criticality. *Phys Rev E* 96:032907.
61. Karmakar S, Lerner E, Procaccia I (2010) Statistical physics of the yielding transition in amorphous solids. *Phys Rev E* 82:055103.
62. Rice JR, Thomson R (1974) Ductile versus brittle behaviour of crystals. *Philos Mag* 29:73–97.
63. Shen J, Huang Y, Sun J (2007) Plasticity of a Ticu-based bulk metallic glass: Effect of cooling rate. *J Mater Res* 22:3067–3074.
64. Kumar G, Neibecker P, Liu YH, Schroers J (2013) Critical fictive temperature for plasticity in metallic glasses. *Nat Commun* 4:1536.
65. Choi IC, et al. (2013) Nanoscale room temperature creep of nanocrystalline nickel pillars at low stresses. *Int J Plasticity* 41:53–64.
66. Schroers J, Johnson WL (2004) Ductile bulk metallic glass. *Phys Rev Lett* 93:255506.